CLOSDI: A Novel Spectral Index for Cloud Shadow Detection in Sentinel-2 Imagery using NDVI and EVI2

Adrián Cal

Instituto Nacional de Investigación Agropecuaria (INIA), Área de Sistemas de Información y Transformación Digital (GRAS), Estación Experimental INIA Las Brujas, Ruta 48 km 10, Rincón del Colorado, 90100, Canelones, Uruguay

ORCID: 0000-0002-2773-0471

e-mail: acal@inia.org.uy

This manuscript has been submitted to a peer-reviewed journal and is currently under review. The content may change before final publication.

ABSTRACT

The presence of clouds and their shadows represents one of the main limitations for the spectral analysis of Sentinel-2 imagery. Although the Scene Classification Layer (SCL), generated by the Sen2Cor algorithm, includes specific classes for cloud shadows and dark area pixels, several studies have revealed limitations in its detection capabilities. This work proposes a new spectral index—the Cloud Shadow Detection Index (CLOSDI)—based on the relationship between NDVI and EVI2, aimed at improving the identification of pixels affected by cloud shadows.

Using the CloudSEN12 dataset as a reference, binary shadow masks were generated from CLOSDI and compared with those provided by the SCL (referred to as S2A-BSM). The optimal CLOSDI Cutoff Threshold (CCT = 35) was determined through an automated process over 3,161 training patches and subsequently applied to an independent test set of 300 patches. The masks were evaluated using standard segmentation metrics: Precision, Recall, F1-Score, IoU, and Balanced Overall Accuracy (BOA).

The masks generated with CLOSDI (CLOSDI-BSM) significantly outperformed those from S2A-BSM across all metrics, achieving a BOA of 76.6 compared to 49.7 for S2A-BSM. When compared to other methods reported in CloudSEN12, CLOSDI-BSM ranked third overall, only behind the Human Level classification and the deep learning-based UNetMobV2 model, and above well-established algorithms such as Fmask, KappaMask, and Sen2Cor.

Unlike these methods, CLOSDI requires no training or GPU usage, and offers a computationally lightweight implementation, making it an effective and accessible tool for cloud shadow detection in Sentinel-2 products, particularly in operational contexts or resource-constrained environments.

Keywords: Cloud shadow detection, Sentinel-2, CLOSDI index, CloudSEN12, Scene Classification Layer (SCL)

1. Introduction

The launch of the Sentinel-2A satellite in June 2015, followed by its twin satellites Sentinel-2B and Sentinel-2C, has sparked a true revolution in the field of remote sensing for Earth observation. As of October 7, 2025, this mission has led to more than 194,000 scientific publications indexed in Google Scholar (search performed using the exact query “Sentinel 2”).

The range of applications for Sentinel-2 is extremely broad and includes studies on ice and glaciers, oceans and seas, rivers and lakes, soil and vegetation, air quality, floods, and wildfires, among others (European Space Agency, n.d.). Some of the key features that explain the mission's success are its global coverage; a spatial resolution of 10 meters for visible and NIR bands and up to 20 meters for red-edge and SWIR bands; a revisit time of 5 days; the acquisition of 13 spectral bands (Copernicus SentiWiki, n.d.); and the ability to calculate hundreds of spectral

indices, such as those compiled in the Awesome Earth Engine Spectral Indices library (Awesome Spectral Indices, n.d.), in addition to being open and freely accessible. It can also be combined with other optical sensors such as Landsat 8 (Claverie et al., 2018).

Despite its many strengths, Sentinel-2 has an inherent limitation common to optical sensors: many of its images contain pixels affected by clouds or their projected shadows, reducing their usefulness in various analyses. To mitigate this problem, the Level-2A product includes, in addition to spectral bands, an additional layer called the Scene Classification Layer (SCL). This band classifies each pixel by land cover (vegetation, water, bare soil, cloud shadow, snow, etc.) and is generated by the Sen2Cor algorithm (Main-Knorn et al., 2017).

The use of the SCL band allows for filtering of unreliable pixels (clouds, shadows, saturated pixels, no data, etc.) and retaining only those suitable for analysis. However, many studies evaluating the utility of SCL for cloud shadow detection have identified several key limitations. The main issues include frequent omission of actual shadows (false negatives), especially over dark surfaces such as water or dense vegetation; false positives where shadows are confused with water bodies or other dark areas; poor performance in complex scenes with thin clouds or low illumination; and strong dependence on the quality of cloud detection, since errors in cloud identification directly affect the location of their shadows (Domnich et al., 2021; Layton et al., 2023; Li et al., 2022; Liang et al., 2024; Raiyani et al., 2021; Tarrio et al., 2020; Wright et al., 2024; Zekoll et al., 2022).

The presence of shadows significantly alters reflectance across all spectral bands, affecting the calculation of indices such as SAVI or EVI, and can lead to misinterpretations or spurious results in models or classifications. Since the problem of shadows affects image analysis regardless of region or application, it is essential to have efficient methods for their detection and filtering.

This study proposes a new normalized spectral index, constructed from the relationship between NDVI and EVI2, aimed at more accurately detecting pixels affected by shadows. This index would complement the filtering performed by Sen2Cor, which primarily uses blue, NIR, and SWIR bands for cloud and shadow detection. Unlike conventional approaches, the proposed index relies exclusively on visible and NIR bands, making it especially useful in scenes where SWIR bands are noisy or unavailable.

Applying this index would enable the generation of more accurate and consistent shadow masks, reducing both false negatives and false positives produced by the SCL algorithm. This would improve the quality of Sentinel-2 derived products such as vegetation time-series, land cover maps, phenological models, and agricultural productivity analyses. Moreover, due to its ease of implementation in platforms like Google Earth Engine, it could be integrated into automated processing pipelines, facilitating large-scale use in environmental monitoring, precision agriculture, or climate change studies.

Additionally, its spectral index-based approach would allow for potential adaptation to similar sensors such as Landsat 8/9 and MODIS, broadening its applicability beyond the Copernicus program. In this regard, the proposed index represents a versatile, replicable, and computationally inexpensive tool to mitigate one of the main challenges of optical remote sensing: interference caused by cloud-projected shadows.

2. Materials & methods

2.1. CloudSEN12

The development of data science and machine learning solutions requires, as a fundamental condition, access to high-quality data, which serves as the essential input for model training. However, in many cases, the necessary data is not publicly available, and in others, it simply does not exist.

The aim of this study was to improve the detection of cloud shadow areas in Sentinel-2 imagery. To this end, a publicly available dataset called CloudSEN12 (CS12) was used, which contains Sentinel-2 images annotated with cloud and cloud shadow labels.

CS12 is a global dataset specifically designed to enhance the semantic segmentation of clouds and shadows in Sentinel-2 imagery, supporting the development and evaluation of different

algorithms. Unlike other datasets, CS12 includes more than 49,000 image patches from various geographic regions, with different levels of cloud cover, allowing for the capture of a wide range of atmospheric conditions and surface types (Aybar et al., 2022).
The CS12 images combine data from Sentinel-2 (Levels 1C and 2A), Sentinel-1, digital elevation models, land cover maps, and water bodies, providing a robust contextual basis for classification tasks. Each patch covers an area of 5,090 × 5,090 meters. The annotations were made by 14 experts using interactive tools and active learning techniques, resulting in high-quality pixel-level labels, as well as partial annotations (scribbles) in some cases. The semantic categories included in CS12 are four: Clear, Thick Cloud, Thin Cloud, and Cloud Shadow (Table 1).

Table 1 Semantic categories defined in the CloudSEN12 dataset.

Code	Category	Description
0	Clear	Pixels without cloud and cloud shadow contamination.
1	Thick Cloud	Opaque clouds that block all the reflectance from the Earth's surface.
2	Thin Cloud	Semitransparent cloud that alters the surface spectral signal but still allows to recognize the background.
3	Cloud Shadow	Dark pixels thrown by a thick or thin cloud.

The dataset can be freely downloaded via the Python package cloudsen12 (pypi.org/project/cloudsen12) or from its official website (cloudsen12.github.io), where example scripts and pretrained models for PyTorch are also provided. The images are organized in optimized GeoTIFF (COG) format and accompanied by STAC metadata, facilitating their integration into automated satellite image processing workflows.
The processing of CS12 patches and Sentinel-2A (S2A) imagery was conducted using Python on the Google Colaboratory platform (colab.google), also known as Google Colab. This free, cloud-based platform allows users to write and execute Python code directly from a browser without installing additional software. It is particularly suited for data analysis, machine learning, and deep learning tasks, offering access to GPUs and TPUs. Through interactive notebooks like Jupyter, it supports the integration of code, visualizations, and Markdown documentation. Its compatibility with Google Drive also enables real-time editing and collaboration. In the field of remote sensing, it is frequently used in combination with Google Earth Engine for downloading, analyzing, and processing satellite imagery.
To access the CS12 patches and their corresponding Sentinel-2 images, Google Earth Engine (earthengine.google.com) was used and accessed through Google Colab. This platform provides planetary-scale geospatial analysis capabilities, enabling the processing and visualization of large volumes of satellite data without the need for local infrastructure. Google Earth Engine offers access to an extensive catalog of imagery and environmental variables, along with advanced analytical tools via JavaScript and Python interfaces, and is widely used in studies on climate change, deforestation, agriculture, water management, and environmental monitoring (Gorelick et al., 2017).
The satellite figures presented throughout this study were generated using QGIS 3.28.11-Firenze.

The CS12 dataset is structured into three annotation levels:

(i) High quality: 10,000 images with full pixel-level labels.
(ii) Scribble: 10,000 images annotated using quick strokes or sketch-like labels.
(iii) Unlabeled: 29,400 images without manual annotations.

Each image, or Image Patch (IP), represents a geographic region with varying levels of cloud cover. For each Region of Interest (ROI), five IPs are included corresponding to different atmospheric conditions: cloud-free (0%), almost clear (0–25%), low cloudiness (25–45%), medium cloudiness (45–65%), and heavily clouded (>65%). This stratification ensures both temporal and spatial variability, which is essential for training and validating cloud and shadow

detection algorithms. Fig. 1 shows an example of an IP along with its corresponding semantic categories.

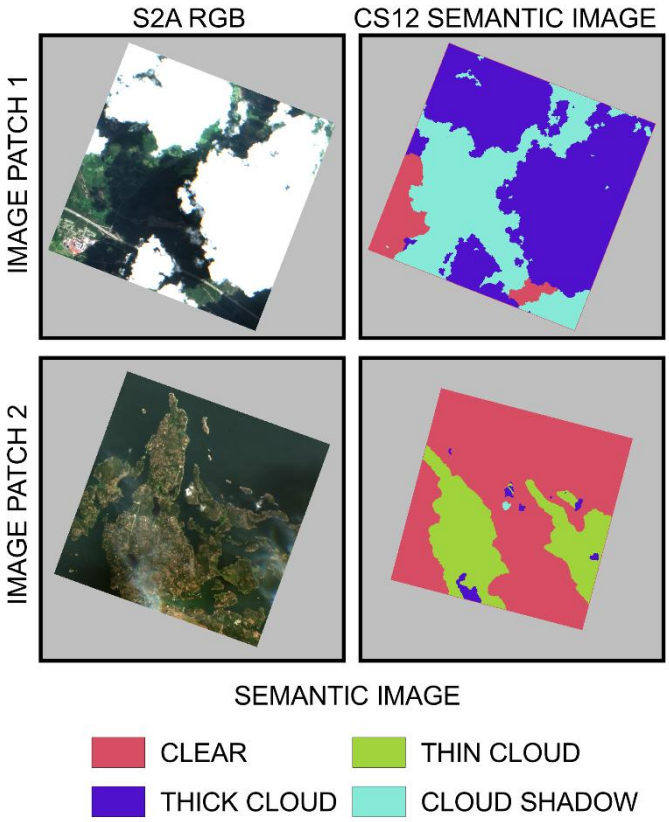

Fig. 1. Example of CloudSEN12 patches with RGB images and semantic segmentation.

For this study, only high-quality patches were selected, that is, those with complete pixel-level annotations. From these, only those with low (25–45%) and medium (45–65%) cloud cover were selected, discarding both cloud-free and almost clear scenes—due to the absence of shadows—as well as heavily clouded ones, where clear areas are minimal. This selection ensures that the images used contain both clear and cloud-affected areas, which is essential for a robust evaluation of the proposed methodology. Out of the 10,000 high-quality patches available, a total of 3,461 were selected for training (see Fig. 2).

The methodology developed in this study requires the use of binary images called Binary Shadow Masks (BSM), in which pixels are classified into two categories: cloud shadow (1) and non-cloud shadow (0). Since the Semantic Images (SI) from CS12 contain four possible values (see Table 1), it was necessary to convert them into binary images. For this, pixels with values 0, 1, and 2 (Clear, Thick Cloud, and Thin Cloud) were reassigned to 0, while pixels with value 3 (Cloud Shadow) were reassigned to 1, as illustrated in Fig. 3.

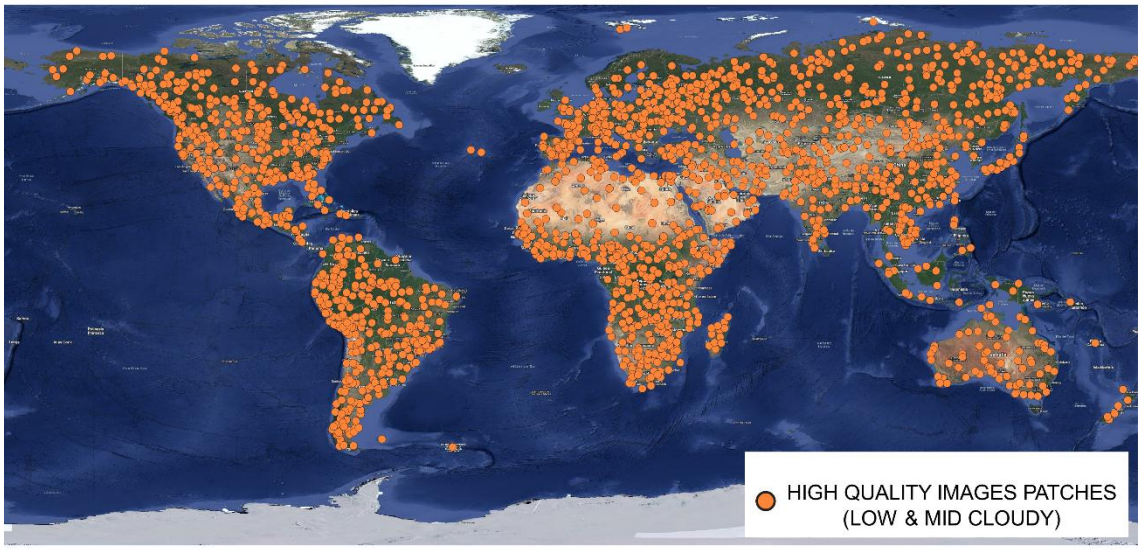

Fig. 2. High-quality patches (low and medium cloud cover) selected from CloudSEN12 for training.

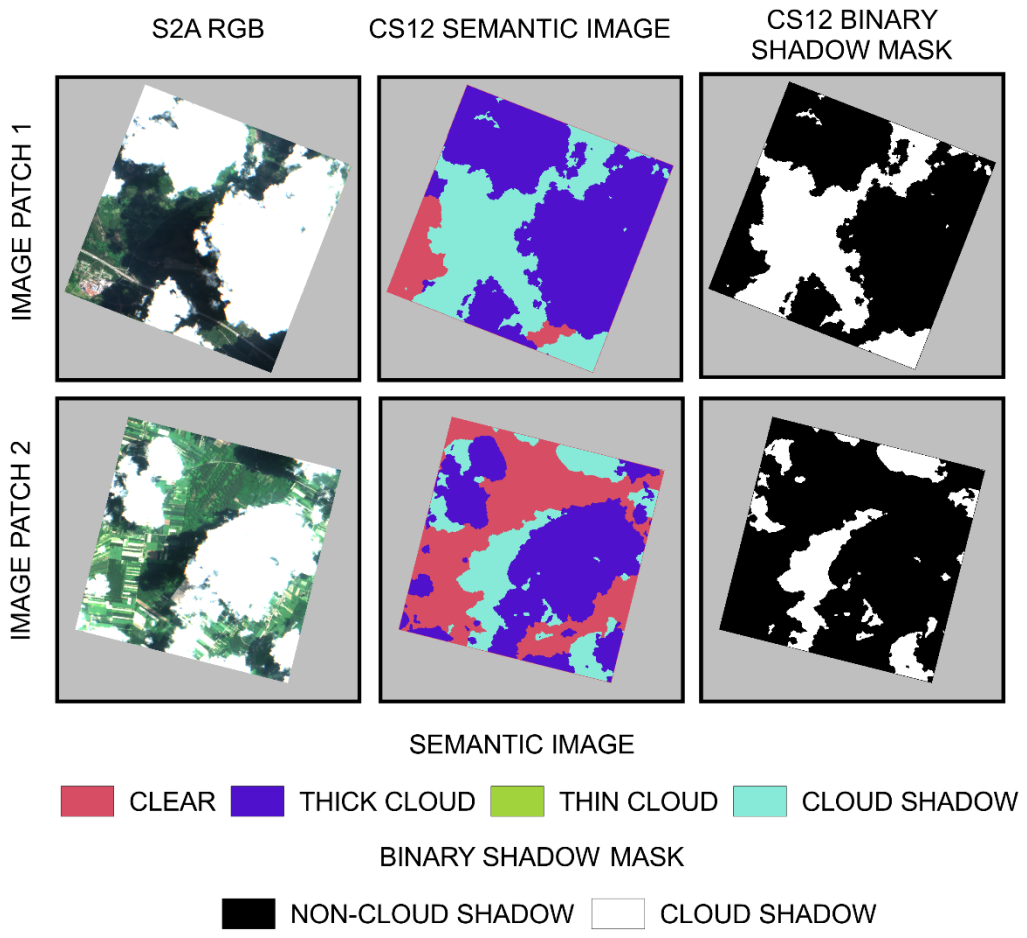

Fig. 3. Conversion of CloudSEN12 semantic images into binary shadow masks (cloud shadow vs. non-cloud shadow).

2.2. Binary shadow mask generation from Sentinel-2A

Since the main objective of this study was to develop a methodology that improves the identification of cloud shadows compared to the detection provided by S2A, it was necessary to evaluate the performance of its Scene Classification Layer (SCL) in shadow detection, using the BSMs generated from CloudSEN12 as reference.

In addition to the standard spectral bands (red, green, near-infrared, etc.), S2A images include the SCL band, which is generated by the Sen2Cor algorithm (Main-Knorn et al., 2017) as part of the atmospheric correction process. This algorithm classifies each pixel into one of 11 different classes, including vegetation, not-vegetated, water bodies, snow, cloud shadows, and various types of clouds (see Table 2). The classification is based on thresholds applied to the top-of-atmosphere (TOA) reflectance values of Sentinel-2's spectral bands, as well as on derived indices such as NDVI and NDSI. The primary purpose of the SCL band is not to map land cover per se, but rather to distinguish usable pixels from those contaminated by atmospheric conditions, thereby facilitating more accurate correction and scientific interpretation of the data.

As with the semantic images from CS12, it was necessary to convert the SCL band into a binary shadow mask (S2A-BSM). In this conversion, pixels belonging to the classes Dark area pixels (2) and Cloud shadows (3) were assigned a value of 1 (cloud shadow), while all other classes were assigned a value of 0 (non-cloud shadow).

For each selected CS12 patch, the corresponding SCL image from S2A was extracted and converted into an S2A-BSM. In this way, comparable shadow mask pairs were generated: one obtained from CS12 (CS12-BSM), and the other from the SCL band of S2A (S2A-BSM).

Fig. 4 shows a representative example of a CS12 patch alongside its S2A RGB image, the CS12 semantic image, the CS12-BSM, the SCL band, and the resulting S2A-BSM after conversion.

Table 2 Description of the classes present in the SCL band of Sentinel-2A (Level-2A).

Code	Class
1	Saturated or defective
2	Dark area pixels
3	Cloud shadows
4	Vegetation
5	Not-vegetated
6	Water
7	Unclassified
8	Cloud medium probability
9	Cloud high probability
10	Thin cirrus
11	Snow/Ice

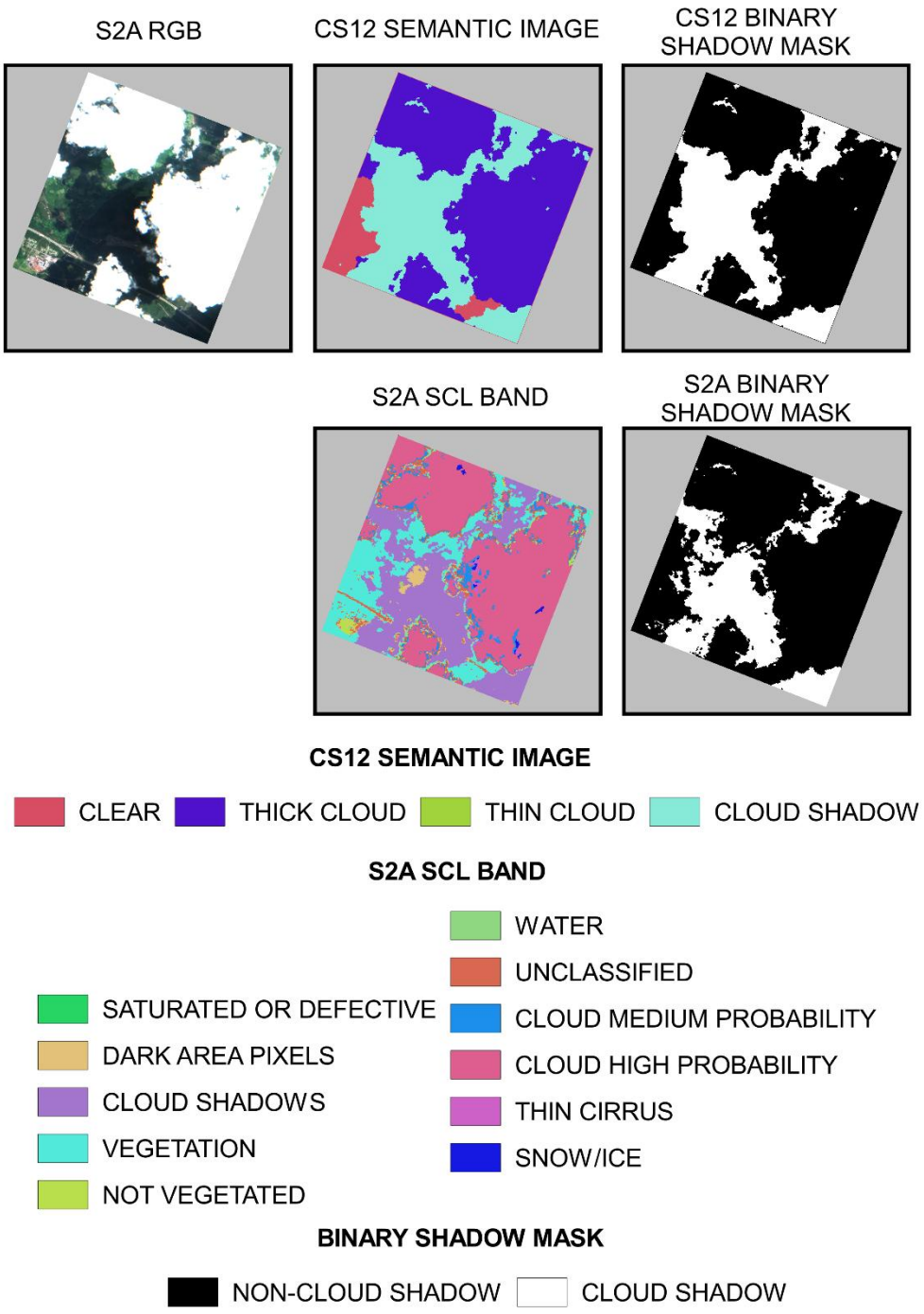

Fig. 4. Conversion of the Sentinel-2A SCL band into a binary shadow mask (S2A-BSM).

2.3. Calculation of EVI2 and NDVI, and formulation of the CLOSDI index

The motivation for developing this study arose from the observation that the SCL band of S2A has limitations in accurately identifying all areas affected by cloud shadows. Fig. 5 shows an example in which the S2A-BSM fails to fully detect the shadow-affected areas, in comparison with the corresponding CS12-BSM.

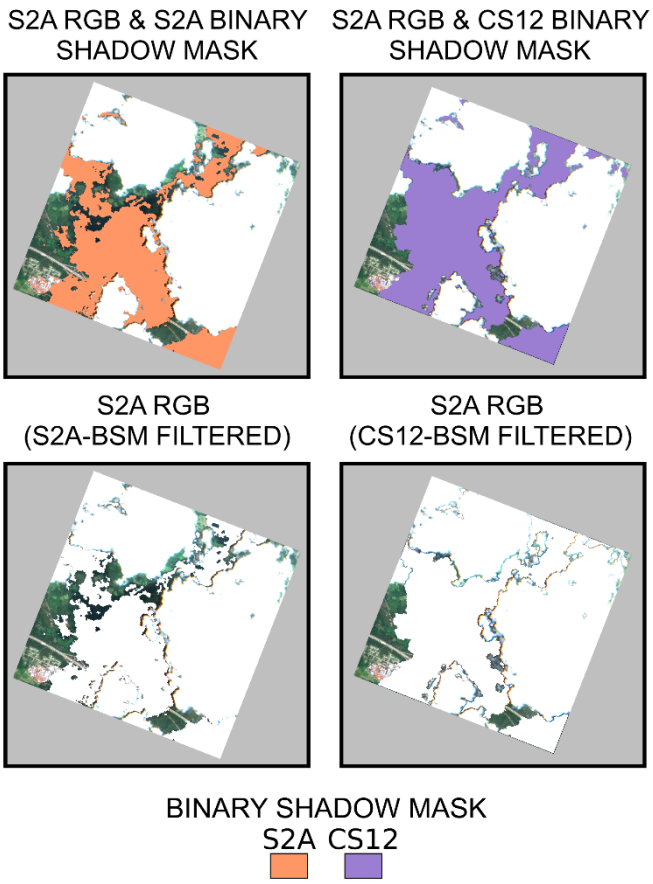

Fig. 5. Comparison between S2A-BSM and CS12-BSM shadow masks in Sentinel-2A images.

When examining some images of the spectral indices Enhanced Vegetation Index (EVI) and Normalized Difference Vegetation Index (NDVI) derived from Sentinel-2A, it was observed that areas affected by cloud shadows tend to exhibit significantly lower EVI values, while NDVI values are less affected in those same areas in comparison to areas without shadows (Fig. 6).
This difference suggests a distinctive behavior between the two indices in the presence of shadows, which led to the central hypothesis of this study: to leverage that difference in order to construct a new index capable of more accurately identifying cloud-shadowed areas, surpassing the detection capabilities provided by the S2A SCL band.
Both EVI and NDVI are calculated from combinations of spectral bands (blue, red, and near-infrared) along with atmospheric correction coefficients (Didan et al., 2015). The equations used are:

$$EVI = G \cdot \frac{(NIR-RED)}{(NIR+C1 \cdot RED-C2 \cdot BLUE+L)} \quad (1)$$

Where the coefficients used are: $C1 = 6$, $C2 = 7.5$, $G = 2.5$, and $L = 1$.

$$NDVI = \frac{(NIR-RED)}{(NIR+RED)} \quad (2)$$

In the case of EVI, the use of the blue band presents challenges due to its high sensitivity to aerosols and other atmospheric contaminants, which complicates atmospheric correction. To overcome these limitations, some authors proposed a simplified version known as EVI2, which omits the blue band but retains the soil-adjustment and linearization properties of the original index (Jiang et al., 2008).

The equation is:

$$EVI2 = G \cdot \frac{(NIR-RED)}{(NIR+C)\cdot(RED+L)} \quad (3)$$

With $C = 2.4$, $G = 2.5$, and $L = 1$.

Since EVI2 does not require the blue band and is simpler to implement, it was selected for use in this study. Prior to developing the new index, an exhaustive search was conducted to determine whether any existing index combined EVI/EVI2 and NDVI. Several sources were consulted, including:

- The standardized Awesome Spectral Indices (ASI) catalog: https://awesome-ee-spectral-indices.readthedocs.io/en/latest/index.html, which compiles over 230 indices used in Earth system studies (Awesome Spectral Indices, n.d.).
- The Sentinel Hub index database: https://custom-scripts.sentinel-hub.com/custom-scripts/sentinel-2/indexdb.
- The Google Scholar search engine.
- The Deep Research tool by OpenAI: https://openai.com/index/introducing-deep-research.

None of these resources contained an index with the following equation:

$\frac{NDVI-EVI}{NDVI+EVI}$ or $\frac{NDVI-EVI2}{NDVI+EVI2}$

Therefore, a new index is proposed, called the Cloud Shadow Detection Index (CLOSDI), whose equation is:

$$CLOSDI = \frac{(NDVI-EVI2)}{(NDVI+EVI2)} \cdot 100 \quad (4)$$

Since both EVI2 and NDVI can take negative values, modified versions of both indices were defined to restrict their values to the [0, 1] range, which facilitates their use in the interpretation of the proposed index. This modification is performed by assigning a value of 0 to any negative value:

$$EVI2mod = max\,(0, EVI2) \quad (5)$$

$$NDVImod = max\,(0, NDVI) \quad (6)$$

With these modified versions, the adjusted equation of the CLOSDI index is:

$$CLOSDI = \frac{(NDVImod-EVI2mod)}{(NDVImod+EVI2mod)} \cdot 100 \quad (7)$$

For each patch in the training set, the corresponding EVI2 and NDVI images were extracted, and the CLOSDI index was calculated. Fig. 6 shows an example featuring the RGB, EVI2, NDVI, and CLOSDI images for a CS12 patch. In this example, it can be observed that areas affected by cloud shadows exhibit the highest CLOSDI values, reinforcing the utility of the index as a tool for generating binary shadow masks from spectral imagery.

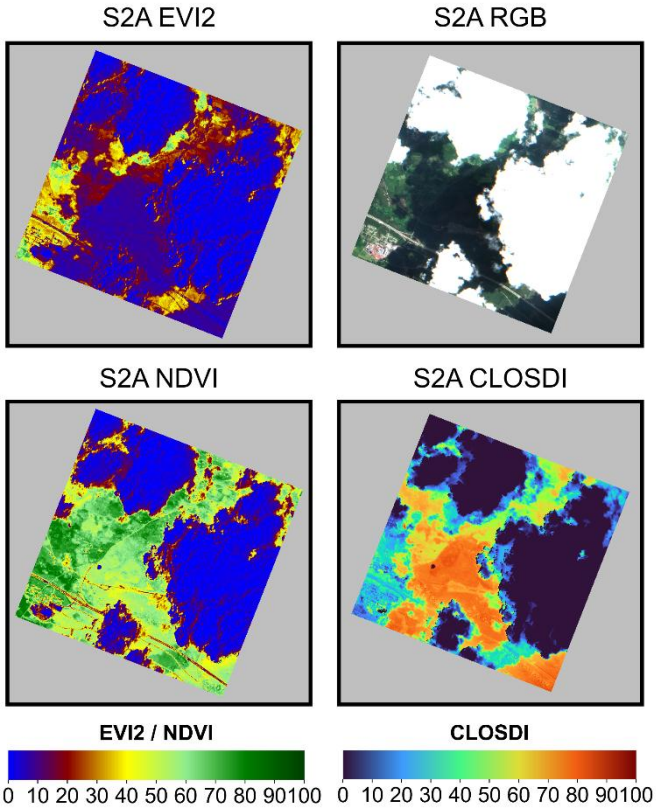

Fig. 6. CloudSEN12 patch with corresponding RGB, EVI2, NDVI, and CLOSDI images.

2.4. Determination of the optimal segmentation threshold for the CLOSDI index

Once the CS12-BSM, S2A-BSM, and the spectral indices EVI2, NDVI, and CLOSDI were obtained for each patch in the training set, the next step was to determine the optimal CLOSDI Cutoff Threshold (CCT). This threshold defines the value above which a pixel is classified as cloud shadow: if the CLOSDI value of a pixel is equal to or greater than the CCT, it is classified as cloud shadow (1); otherwise, as non-cloud shadow (0).

Fig. 7 presents an example of this procedure, where different CCTs (20, 30, 50, and 70) are applied to the same patch. As shown, a low CCT (e.g., 20) tends to overestimate shadow extent, erroneously classifying many areas as shadows. In contrast, a high CCT (e.g., 70) underestimates the shadow extent, omitting many actual shadowed areas. In this case, the optimal CCT appears to fall within the 30 to 50 range.

However, this type of visual adjustment is only feasible for a few cases. For thousands of images, such as those in this study, an automated and quantitative strategy is required.

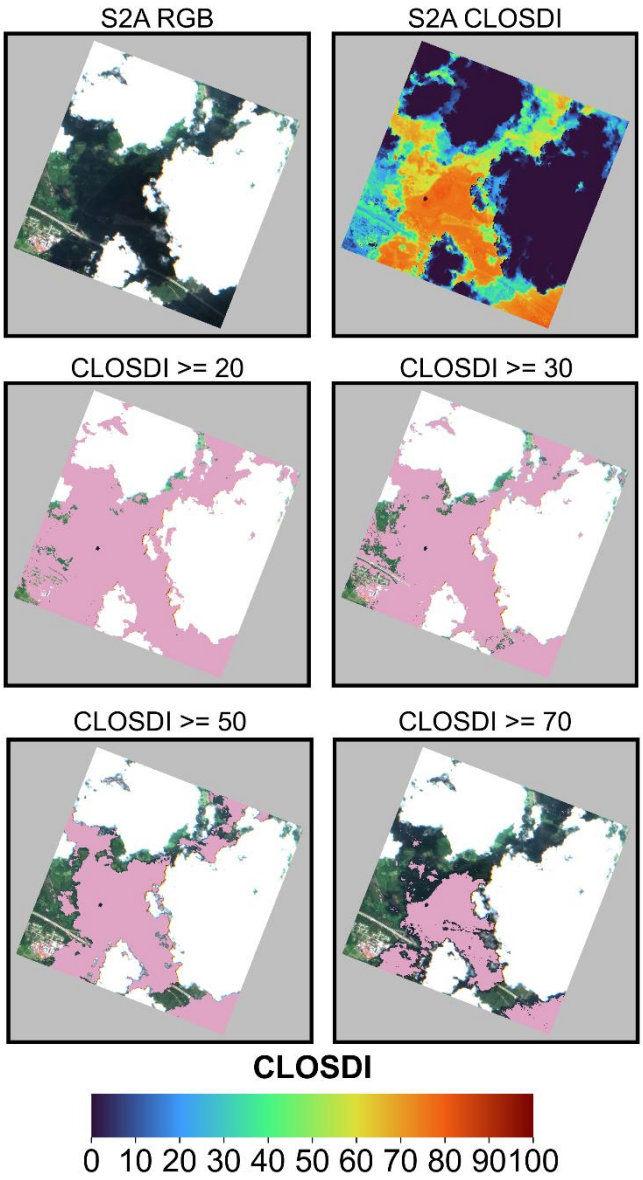

Fig. 7. Visual evaluation of the effect of the CLOSDI cutoff threshold (CCT) on a CloudSEN12 image.

To this end, the set of 3,461 selected patches was divided into two subsets:

- 3,161 patches were used for training and for determining the optimal CLOSDI cutoff threshold.
- The remaining 300 patches were reserved for testing, without being involved in the threshold calibration.

During the training phase, 70 CCT values ranging from 1 to 70 were explored, with one run executed for each value. In each run, 75% of the training set (2,371 patches) was randomly selected, and for each patch, a binary shadow mask was generated from the CLOSDI index using the corresponding CCT.
The validity of each generated mask was quantitatively evaluated using the Jaccard Index, also known as Intersection over Union (IoU). This metric compares the similarity between two sets A and B, and is defined as:

$$J(A,B) = \frac{|A \cap B|}{|A \cup B|} \quad (8)$$

In the context of image segmentation, the Jaccard Index measures the overlap between an automated segmentation (in this case, the mask generated by CLOSDI) and a reference segmentation (CS12-BSM). It is a widely used metric due to its simplicity, computational efficiency, and clear interpretability: a value of 0 indicates no overlap, while a value of 1 indicates a perfect match (da Fontoura Costa, 2021). Fig. 8 illustrates an example of IoU calculation applied to a patch from the training set.

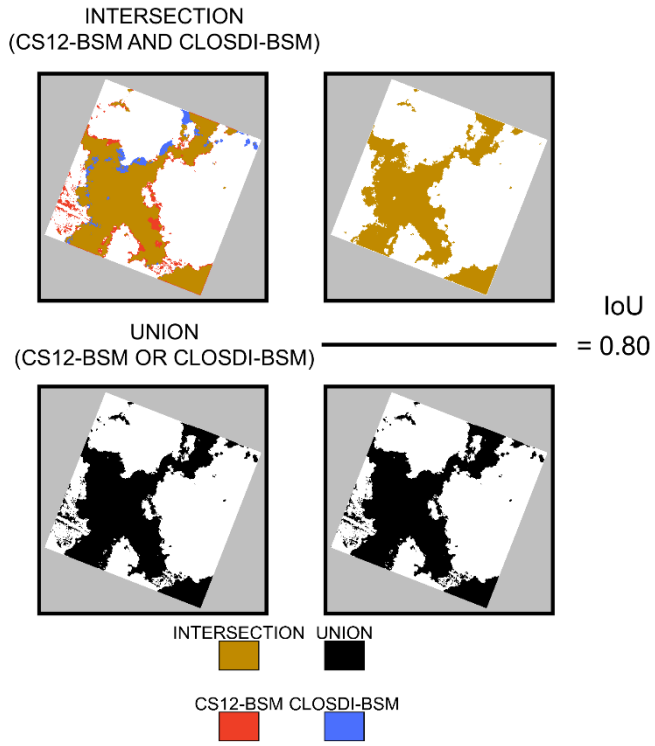

Fig. 8. Illustration of IoU calculation between a CLOSDI-BSM mask and its CS12-BSM reference.

In each run, 2,371 IoU values were calculated (one per patch), scaled by 100 to express them as percentages and facilitate interpretation. The median of these values was used as the performance metric for that CCT. In this way, an IoU vs. CCT performance curve was obtained.
Fig. 9 presents the complete flowchart of the training process and the search for the optimal CCT. The CCT that maximized the IoU was selected as the optimal value for generating masks in the test set.
Finally, to evaluate the ability of the CLOSDI index to detect cloud shadows, five commonly used performance metrics for binary segmentation tasks were applied: Precision, Recall, F1-Score, IoU, and Balanced Overall Accuracy (BOA). The first three metrics were computed following the criteria established in (Sokolova and Lapalme, 2009), while BOA was adopted as defined in the benchmark of the CloudSEN12 dataset (15). These metrics were calculated for both the masks generated using CLOSDI (CLOSDI-BSM) and those generated from the Sentinel-2A SCL band (S2A-BSM). In this way, using the CS12-BSM (based on expert-labeled data) as reference, it was possible to compare the performance of both methodologies. The full workflow of the testing phase is summarized in Fig. 10.

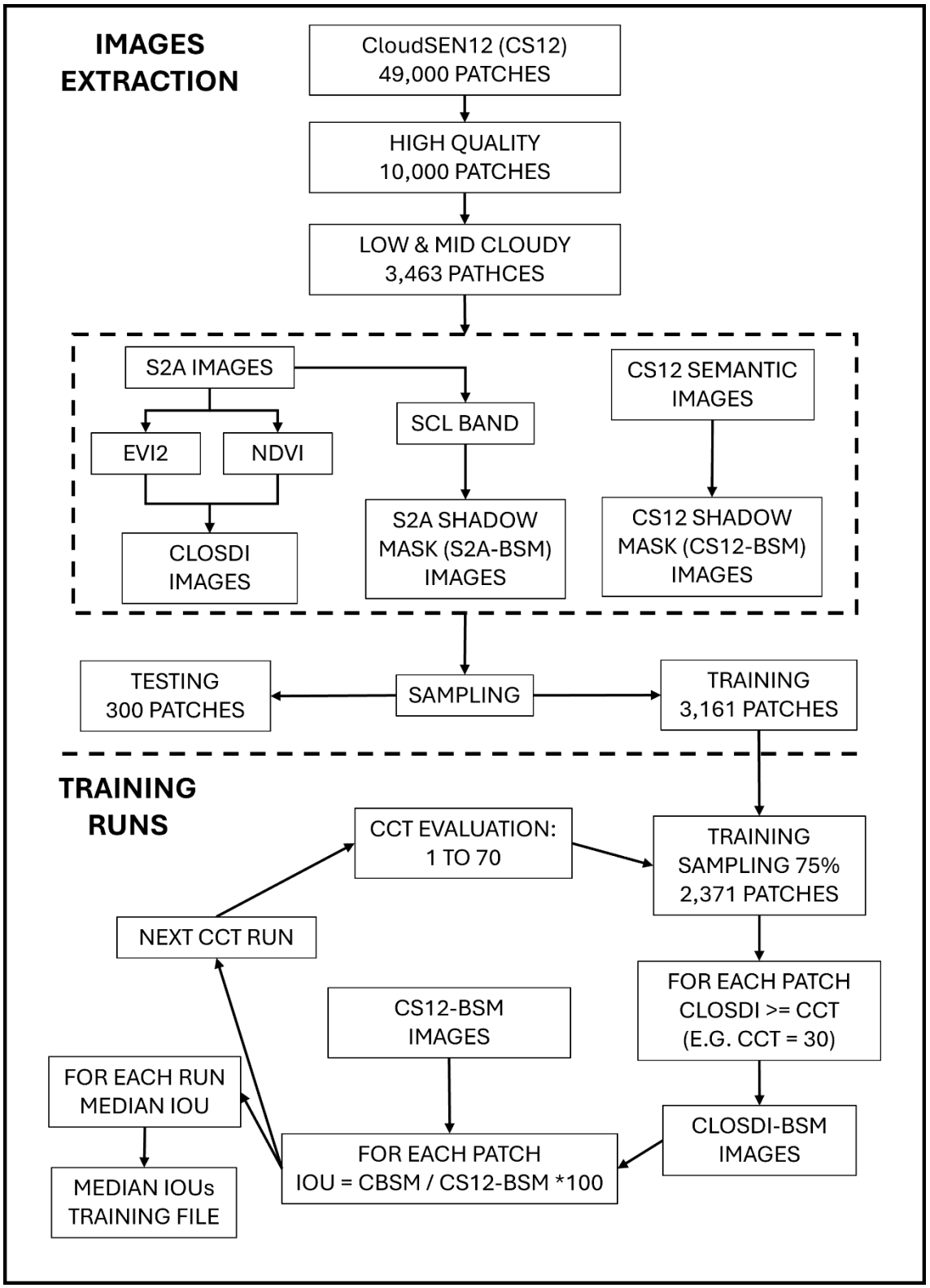

Fig. 9. Flowchart of the training process and selection of the optimal CLOSDI cutoff threshold (CCT).

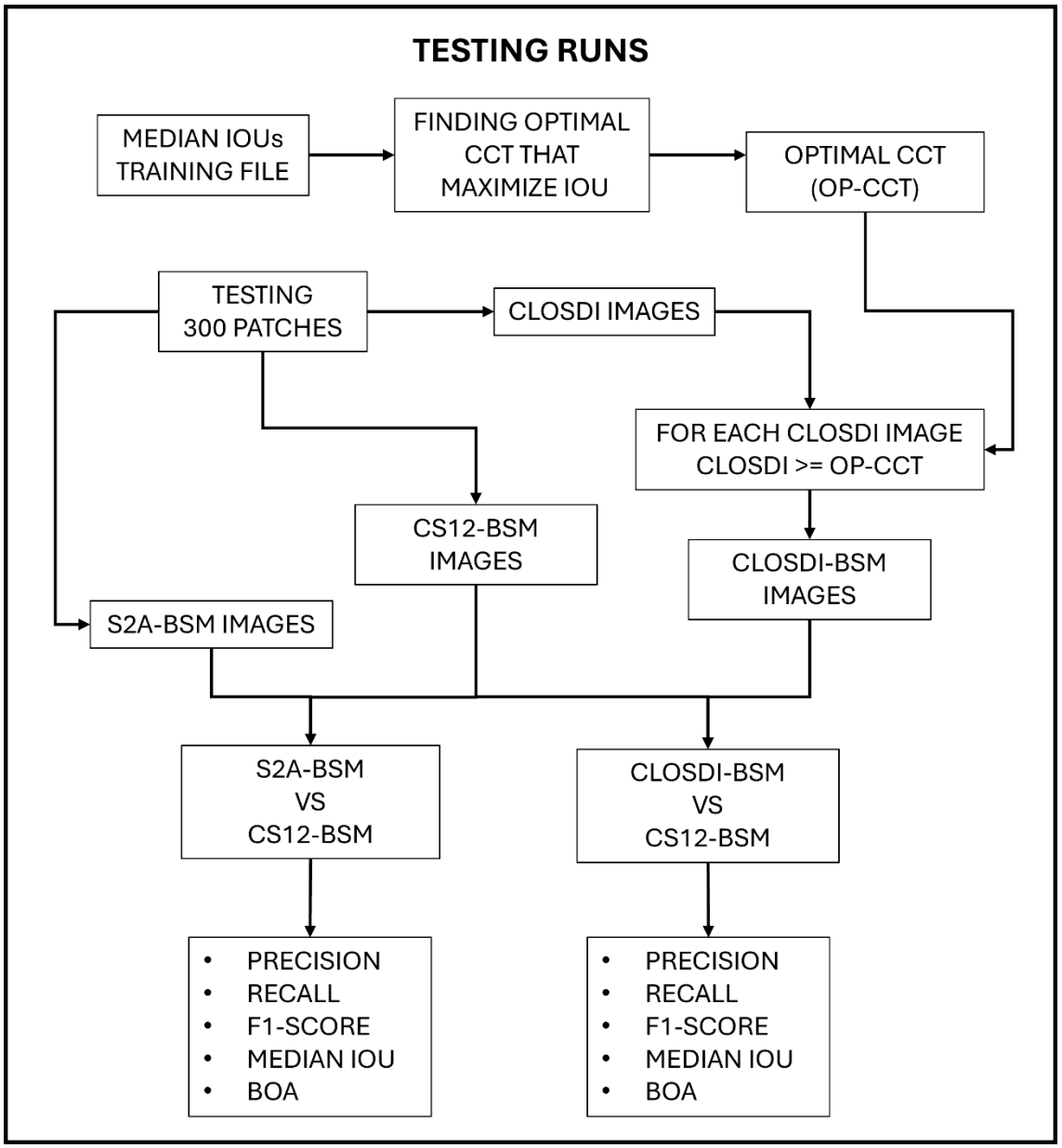

Fig. 10. Flowchart of CLOSDI-BSM performance evaluation on the test set.

3. Results & Discussion

After completing the 70 runs to determine the optimal CCT in the training set, an IoU vs. CCT plot was constructed, as shown in Fig. 11. This plot displays the median IoU values obtained in each run as a function of the corresponding CCT value. In addition, a fitted curve (IoU Fitted) was added based on the observed median IoU values. From this curve, the optimal CCT value that maximized the IoU was identified as 34.3, which corresponded to a maximum IoU of 40.2. As seen in the graph, the IoU increases rapidly from a CCT of 10, reaches its peak at CCT=34.3, and then drops sharply to near-zero values when the CCT exceeds 65.

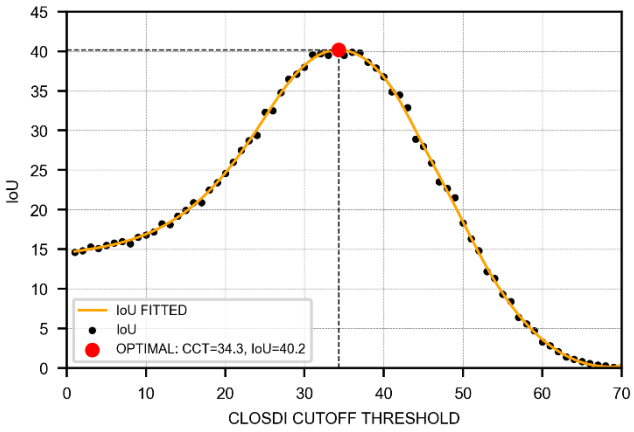

Fig. 11. Performance curve (IoU) as a function of the CLOSDI cutoff threshold (CCT) during training.

For practical purposes in evaluating the quality of the new methodology for detecting cloud shadow areas, the rounded value of the optimal CCT—35—was used. Fig. 12 presents an example of BSMs generated using CLOSDI ≥ 35 for a pair of patches from the test set. For comparison purposes, the corresponding shadow masks provided by S2A (S2A-BSM) for the same images are also included. As can be observed, the shadow mask generated using CLOSDI more accurately identifies areas affected by cloud shadows, visually outperforming the S2A-BSM. This observation supports the usefulness of CLOSDI-BSM as a complementary or alternative tool for shadow detection in Sentinel-2 products.

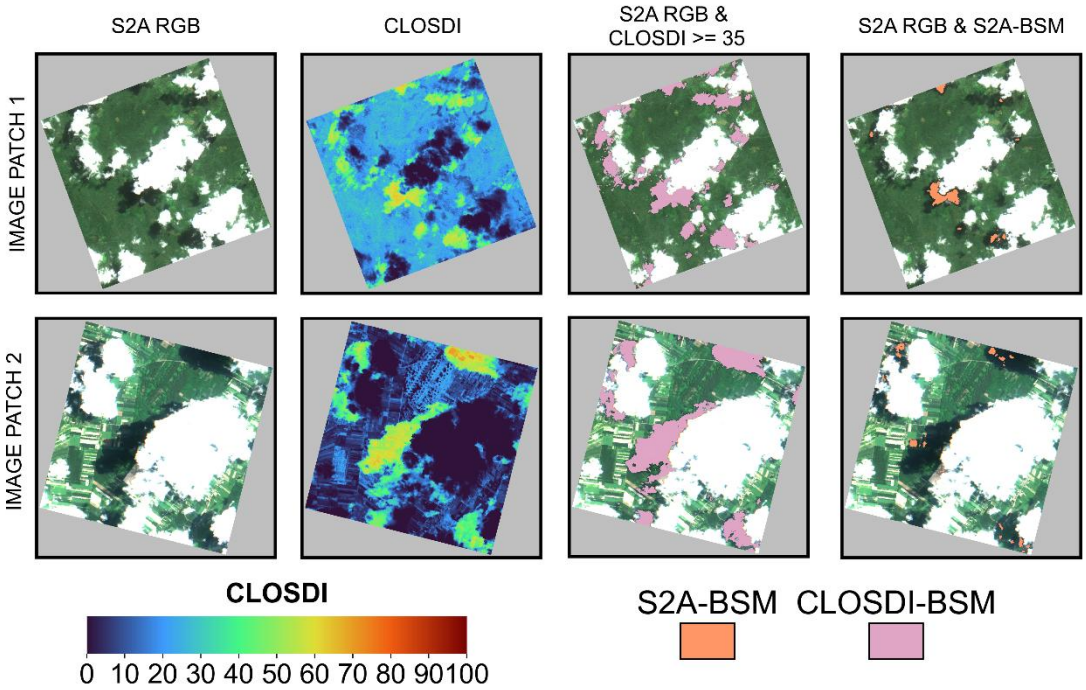

Fig. 12. Comparison between CLOSDI-BSM and S2A-BSM masks for a pair of test set images.

Once the optimal CCT value of 35 was determined, the next step was its evaluation on the set of 300 test patches, following the procedures described in the flowchart in Fig. 10. This process was carried out using the 300 reference CS12-BSM, along with the corresponding S2A-BSM and the new masks generated using the CLOSDI ≥ 35 threshold (CLOSDI-BSM). Both the S2A-BSM and CLOSDI-BSM were compared against the reference CS12-BSM, and the following

performance metrics were calculated: Precision (9), Recall (10), F1-Score (11), IoU, and BOA (12).

$$Precision = \frac{TP}{TP+FP} \quad (9)$$

$$Recall = \frac{TP}{TP+FN} \quad (10)$$

$$F1 - Score = 2 \cdot \frac{P \cdot R}{P+R} \quad (11)$$

$$BOA = 0.5 \cdot (P + R) \quad (12)$$

TP, *FP*, *FN*, *P*, and *R* refer to True Positive, False Positive, False Negative, Precision, and Recall, respectively. The results for the various performance metrics are presented in Fig. 13 and Table 3. As shown, regardless of the metric considered, the performance of CLOSDI-BSM is consistently superior to that of S2A-BSM. Precision reached a value of 65.6 for CLOSDI-BSM, exceeding S2A-BSM (39.2) by 26.4 percentage points. Recall showed an even more pronounced difference: 73.4 for CLOSDI-BSM compared to only 14 for S2A-BSM.

These Recall values indicate, on one hand, that the CLOSDI-based methodology with CCT = 35 has a significantly higher capacity for detecting cloud shadow pixels. On the other hand, the low Recall value of S2A-BSM, combined with its relatively higher Precision, suggests a strong tendency to omit shadow pixels (high false negatives) rather than to overestimate them (high false positives). However, both values are low in absolute terms.

In contrast, CLOSDI-BSM shows more balanced Precision and Recall values, indicating a more even performance between omission and overestimation. Nonetheless, the fact that Recall exceeds Precision by 7.8 points suggests a slight tendency to overestimate shadows rather than miss them—although the difference is not substantial.

As a result of these values, the F1-Score for CLOSDI-BSM reaches 57.8, far higher than the 20.6 observed for S2A-BSM. Similarly, the IoU (40.6 vs. 14.6) and BOA (76.6 vs. 49.7) metrics further reinforce the superior overall performance of CLOSDI-BSM compared to S2A-BSM.

Table 3 Performance metric results for CLOSDI-BSM and S2A-BSM on the test set.

METRIC	CLOSDI-BSM	S2A-BSM
PRECISION	65.6	39.2
RECALL	73.4	14
F1-SCORE	57.8	20.6
IOU	40.6	14.6
BOA	76.6	49.7

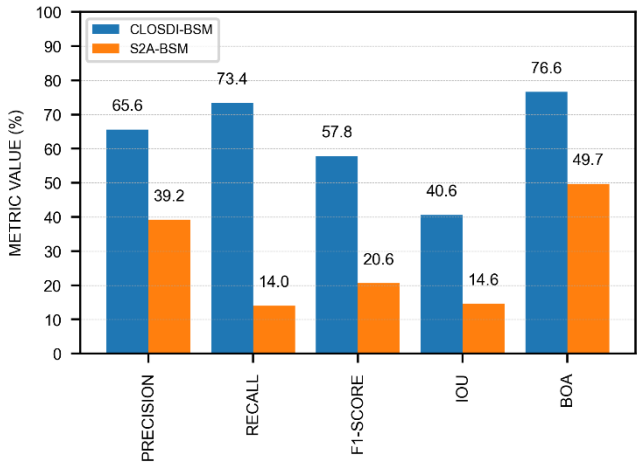

Fig. 13. Comparison of performance metrics between CLOSDI-BSM and S2A-BSM on the test set.

Finally, Table 4 and Fig. 14 compare the BOA values obtained in this study for CLOSDI-BSM and S2A-BSM with those reported in the CloudSEN12 study (expressed as percentages). As shown, the methodology developed in this work ranks third overall, surpassed only by Human Level classification (performed by human experts) and the UNetMobV2 methodology (Aybar et al., 2022), which is based on deep learning.

The CLOSDI-based methodology achieves performance comparable to, and even slightly better than, KappaMask L1C (Domnich et al., 2021) and Fmask (Qiu et al., 2019). In contrast, S2A-BSM yielded the worst performance among the compared methods, with a BOA value very similar to Sen2Cor, the algorithm used by Sentinel-2A to generate the SCL band, from which the S2A-BSM used in this study were derived. Additionally, the CLOSDI methodology outperformed KappaMask L2A (Domnich et al., 2021) by 12.6 percentage points.

It is worth noting that the proposed methodology in this study presents significantly lower complexity compared to the algorithms evaluated in CloudSEN12. By ranking second overall—excluding Human Level classification—one of its main strengths becomes evident: its implementation requires considerably fewer computational resources, does not depend on GPU usage like KappaMask and UNetMobV2, and is simpler than both Sen2Cor and Fmask.

Table 4 Comparison of BOA between CLOSDI-BSM, S2A-BSM, and benchmark algorithms from CloudSEN12.

ALGORITHM	TYPE	BOA
Human level	Human expert labeling.	99
UNetMobV2	Deep learning based on U-Net with MobileNetV2 backbone.	89
CLOSDI-BSM	Spectral index with fixed threshold.	76.6
KappaMask L1C	Deep learning with U-Net architecture.	74
Fmask	Deterministic, based on physical rules and spectral thresholds.	72
KappaMask L2A	Deep learning with U-Net architecture.	64
Sen2Cor	Deterministic, based on rules and physical thresholds.	51
S2A-BSM	Based on the SCL band from Sen2Cor.	49.7

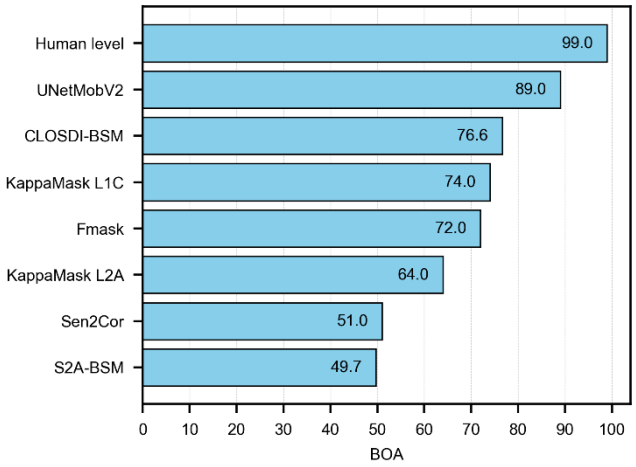

Fig. 14. BOA comparison between CLOSDI-BSM, S2A-BSM, and benchmark algorithms from CloudSEN12.

4. Conclusions

In this study, a new spectral index called CLOSDI (Cloud Shadow Detection Index) was developed and validated. Based on the relationship between EVI2 and NDVI, this index aims to improve the detection of cloud shadows in Sentinel-2 imagery. The index was evaluated using the CloudSEN12 dataset, which provides expert-labeled shadow masks widely used as a reference in the scientific community.

From the analysis of 3,161 training patches, an optimal CLOSDI cutoff threshold (CCT) of 35 was identified. Using this threshold, binary shadow masks (CLOSDI-BSM) were generated and applied to an independent test set of 300 patches. These masks were compared against those provided by the SCL classification band from Sentinel-2 (S2A-BSM), using five standard metrics: Precision, Recall, F1-Score, IoU, and BOA.

The results indicate that CLOSDI-BSM consistently outperformed S2A-BSM across all metrics, particularly in Recall (73.4 vs. 14) and BOA (76.6 vs. 49.7), demonstrating a greater ability to correctly identify cloud-shadowed pixels, with a good balance between omissions and overestimations. Furthermore, when comparing BOA values with other methods evaluated in the CloudSEN12 study, CLOSDI-BSM ranked third overall, only behind Human Level classification and the deep learning-based UNetMobV2 model, and ahead of well-established algorithms such as Fmask, KappaMask L1C/L2A, and Sen2Cor.

One of the main advantages of the proposed methodology is its low computational complexity. Unlike KappaMask and UNetMobV2, which require GPU-based training and deep network architectures, CLOSDI does not require any training or specialized infrastructure, making it a particularly useful alternative in resource-constrained environments or in contexts that demand fast and reproducible processing.

In summary, CLOSDI represents an efficient, simple, and highly competitive solution for cloud shadow detection in Sentinel-2 products. It can be used as a complementary or substitute tool for more complex methods in operational environmental monitoring and multitemporal spectral analysis applications.

Future research directions include extending the application of CLOSDI to other satellite missions such as Landsat and MODIS, integrating it into automated pipelines for large-scale time-series analyses, and combining it with machine learning-based post-processing techniques to further enhance its accuracy and broaden its applicability in operational and research contexts.

Conflict of Interest

The author declares no conflict of interest.

Funding sources

This research did not receive any specific grant from funding agencies in the public, commercial, or not-for-profit sectors. The work was carried out as part of the author's regular activities at the Instituto Nacional de Investigación Agropecuaria (INIA, Uruguay).

Data availability

All data used in this work come from published and open-access sources and are fully attributed. Sentinel-2 imagery was accessed via the Google Earth Engine platform (https://earthengine.google.com), and the CloudSEN12 benchmark dataset (Aybar et al., 2022) was used for validation and is publicly available at https://cloudsen12.github.io/

Author Contribution

The author performed all aspects of the research, including conceptualization, methodology, data analysis, programming, validation, visualization, and writing of the manuscript.

Acknowledgements

The author gratefully acknowledges the institutional support of the Instituto Nacional de Investigación Agropecuaria (INIA, Uruguay) and the availability of open-access resources such as the Google Earth Engine platform and the CloudSEN12 project (https://cloudsen12.github.io/), which made this research possible. The author also thanks the remote sensing research community for their continuous efforts in promoting open and reproducible science.

References

Awesome Spectral Indices, n.d. Awesome Earth Engine Spectral Indices [WWW Document]. URL https://awesome-ee-spectral-indices.readthedocs.io/en/latest/index.html

Aybar, C., Ysuhuaylas, L., Loja, J., Gonzales, K., Herrera, F., Bautista, L., Yali, R., Flores, A., Diaz, L., Cuenca, N., Espinoza, W., Prudencio, F., Llactayo, V., Montero, D., Sudmanns, M., Tiede, D., Mateo-García, G., Gómez-Chova, L., 2022. CloudSEN12, a global dataset for semantic understanding of cloud and cloud shadow in Sentinel-2. Sci. Data 9, 782. https://doi.org/10.1038/s41597-022-01878-2

Claverie, M., Ju, J., Masek, J.G., Dungan, J.L., Vermote, E.F., Roger, J.-C., Skakun, S. V., Justice, C., 2018. The Harmonized Landsat and Sentinel-2 surface reflectance data set. Remote Sens. Environ. 219, 145–161. https://doi.org/10.1016/j.rse.2018.09.002

Copernicus SentiWiki, n.d. Sentinel-2 Mission [WWW Document]. URL https://sentiwiki.copernicus.eu/web/s2-mission

da Fontoura Costa, L., 2021. Further generalizations of the Jaccard index, arXiv preprint arXiv:2110.09619.

Didan, K., Munoz, A.B., Solano, R., Huete, A., 2015. MODIS vegetation index user's guide (MOD13 series), University of Arizona: Vegetation Index and Phenology Lab.

Domnich, M., Sünter, I., Trofimov, H., Wold, O., Harun, F., Kostiukhin, A., Järveoja, M., Veske, M., Tamm, T., Voormansik, K., Olesk, A., Boccia, V., Longepe, N., Cadau, E.G., 2021. KappaMask: AI-Based Cloudmask Processor for Sentinel-2. Remote Sens. 13, 4100. https://doi.org/10.3390/rs13204100

European Space Agency, n.d. Sentinel success stories [WWW Document]. URL https://sentinel.esa.int/web/success-stories/list

Gorelick, N., Hancher, M., Dixon, M., Ilyushchenko, S., Thau, D., Moore, R., 2017. Google Earth Engine: Planetary-scale geospatial analysis for everyone. Remote Sens. Environ. 202, 18–27. https://doi.org/10.1016/j.rse.2017.06.031

Jiang, Z., Huete, A., Didan, K., Miura, T., 2008. Development of a two-band enhanced vegetation index without a blue band. Remote Sens. Environ. 112, 3833–3845.

https://doi.org/10.1016/j.rse.2008.06.006
Layton, J.C., Wecker, L., Runions, A., Samavati, F.F., 2023. Cloud Shadow Detection via Ray Casting with Probability Analysis Refinement Using Sentinel-2 Satellite Data. Remote Sens. 15, 3955. https://doi.org/10.3390/rs15163955
Li, Z., Shen, H., Weng, Q., Zhang, Y., Dou, P., Zhang, L., 2022. Cloud and cloud shadow detection for optical satellite imagery: Features, algorithms, validation, and prospects. ISPRS J. Photogramm. Remote Sens. 188, 89–108. https://doi.org/10.1016/j.isprsjprs.2022.03.020
Liang, K., Yang, G., Zuo, Y., Chen, J., Sun, W., Meng, X., Chen, B., 2024. A Novel Method for Cloud and Cloud Shadow Detection Based on the Maximum and Minimum Values of Sentinel-2 Time Series Images. Remote Sens. 16, 1392. https://doi.org/10.3390/rs16081392
Main-Knorn, M., Pflug, B., Louis, J., Debaecker, V., Müller-Wilm, U., Gascon, F., 2017. Sen2Cor for Sentinel-2, in: Bruzzone, L., Bovolo, F., Benediktsson, J.A. (Eds.), Image and Signal Processing for Remote Sensing XXIII. SPIE, p. 3. https://doi.org/10.1117/12.2278218
Qiu, S., Zhu, Z., He, B., 2019. Fmask 4.0: Improved cloud and cloud shadow detection in Landsats 4–8 and Sentinel-2 imagery. Remote Sens. Environ. 231, 111205. https://doi.org/10.1016/j.rse.2019.05.024
Raiyani, K., Gonçalves, T., Rato, L., Salgueiro, P., Marques da Silva, J.R., 2021. Sentinel-2 Image Scene Classification: A Comparison between Sen2Cor and a Machine Learning Approach. Remote Sens. 13, 300. https://doi.org/10.3390/rs13020300
Sokolova, M., Lapalme, G., 2009. A systematic analysis of performance measures for classification tasks. Inf. Process. Manag. 45, 427–437. https://doi.org/10.1016/j.ipm.2009.03.002
Tarrio, K., Tang, X., Masek, J.G., Claverie, M., Ju, J., Qiu, S., Zhu, Z., Woodcock, C.E., 2020. Comparison of cloud detection algorithms for Sentinel-2 imagery. Sci. Remote Sens. 2, 100010. https://doi.org/10.1016/j.srs.2020.100010
Wright, N., Duncan, J.M.A., Callow, J.N., Thompson, S.E., George, R.J., 2024. CloudS2Mask: A novel deep learning approach for improved cloud and cloud shadow masking in Sentinel-2 imagery. Remote Sens. Environ. 306, 114122. https://doi.org/10.1016/j.rse.2024.114122
Zekoll, V., de los Reyes, R., Richter, R., 2022. A Newly Developed Algorithm for Cloud Shadow Detection—TIP Method. Remote Sens. 14, 2922. https://doi.org/10.3390/rs14122922